Hybrid smith predictor-neuroendocrine control for semi-active suspension of high-clearance agricultural sprayers

Congcong Chen[1], Weiwei Song[2], Gang Li[3], Yuling Ye[4], Junfeng An[5]
[1, 4]The Key Laboratory of Road and Traffic Engineering, Ministry of Education, Tongji University, Shanghai, China
[1, 4]College of Transportation, Tongji University, Shanghai, China
[1]School of Rail Transportation, Shandong Jiaotong University, Jinan, China
[3, 5]Jinan Railway Transportation Group Co, Ltd, Jinan, China
[2]College of Science and Technology, Ningbo University, Ningbo, China
[1]Corresponding author
E-mail: [1]*215003@sdjtu.edu.cn*, [2]*songweiwei2@nbu.edu.cn*, [3]*gang.li@live.cn*, [4]*yyling71@163.com*, [5]*97098541@qq.com*

Received 15 December 2025; accepted 7 April 2026; published online 16 May 2026
DOI https://doi.org/10.21595/jve.2026.25916

Abstract. . In order to attain time-lag dynamic compensation control and decrease time-lag influence of high-clearance sprayer semi-active suspensions, a novel suspension intelligent controller based on improved Smith prediction neuroendocrine algorithm is proposed. Firstly, the time-lag semi-active suspension dynamic model of high-clearance sprayers is established, the neuroendocrine intelligent controller is designed combined with the hormone regulation mechanism in the organism. Then, by combining enhanced Smith prediction compensation controller with neuroendocrine intelligent controller, a kind of high-clearance sprayer semi-active suspension intelligent controller based on the improved Smith prediction neuroendocrine algorithm is developed. The research results show the proposed algorithm can significantly reduce body vertical acceleration (BVA) and tire dynamic load (TDL) indicators of high-clearance sprayer semi-active suspensions, effectively improve smoothness and road friendliness of sprayers, significantly enhance comprehensive performance, show strong adaptability and robustness under working conditions, and is very suitable for vibration control of the high-clearance sprayer semi-active suspension with high order time-varying, complex nonlinear and strong coupling.

Keywords: high-clearance sprayer, time-lag, smith prediction, neuroendocrine, semi-active suspension.

1. Introduction

High-clearance self-propelled sprayer, as a key agricultural equipment in plant protection operation, plays a crucial role in maintaining food production safety and agricultural stable development [1]. The working environment of high-clearance sprayer is mostly bumpy and uneven field road, and the body is prone to produce large vibration, which affects the driving stability and ride comfort of the sprayer. In addition, the vibration of the body will couple with the spray bar of the sprayer, which will make the spray bar vibration more intense, damage the spray bar, and seriously affect the spray quality of the sprayer [2]. Suspension system is a crucial equipment of high-clearance self-propelled sprayers, which can effectively dampen vibration shocks of high-clearance sprayers from the ground, reduce vibration of body and spray bar, ensure spray accuracy of sprayers and extend the life of the spray bar. Therefore, it is of great importance to enhance spraying effect, ride comfort and road-friendliness of high-clearance sprayers.

At present, most of heavy-load high-clearance sprayers developed by mainstream agricultural equipment enterprises at home and abroad use the independent air suspension, which has the

characteristics of large load-carrying, adjustable load capacity and low vibration frequency. However, its cost is high, and it is mainly used in high-end high-clearance sprayer [3, 4]. Most light-load high-clearance sprayer use semi-active suspension with spiral spring and adjustable damping damper, which is characterized by the simple structure, easy installation and realization, and low cost. Domestic and foreign scholars have proposed many control strategies for the suspension system of high-clearance sprayers, such as PID algorithm, fuzzy algorithm, neural network algorithm, robust algorithm, etc. [5-8]. Yin et al. [9] controlled the electromagnetic reversing valve stem from PID method to realize the automatic leveling control of spray bars of high-clearance sprayers, and verified accuracy and stability of spray bar systems in field operation. Xue et al. [10] designed a spray bar active suspension algorithm, which is beneficial for enhancing spray bar operation stability of large high-clearance sprayers. Yang et al [11] proposed a fuzzy neural-network method of high-clearance sprayers, which effectively enhancing the BVA, pitch angle acceleration (PAA) and roll angle acceleration (RAA) indicators of high-clearance sprayers, has good engineering practicability.

Since the 1970s, the theory of biological control has gradually attracted the attention of researchers and developed rapidly. Currently, various biological intelligent controllers have emerged [12-14]. Ding et al. [15] designed a small tracked rapeseed seeder navigation controller on the basis of immune PID controller to address intelligent sowing problem of soil viscosity and small field blocks in rice stubble fields, which can better meet navigation requirements of seeders and provide technical reference for autonomous navigation of tracked seeders. Su et al. [16] designed an airborne real-time variable fertilization control system, which effectively improved uniformity and accuracy of fertilization, thereby enhanced the fertilization performance of centrifugal variable fertilizer spreaders. Jin et al. [17] designed an endocrine intelligent controller based on hormone regulation mechanism of biological endocrine system, proposed a new active suspension endocrine LQR controller combined with traditional linear quadratic regulators, which has excellent quality, good adaptability to changing operating parameters, and better vibration reduction effect than traditional LQR controllers. The regulation of various hormones by neuroendocrine system has the advantages of better adaptivity and stability, etc. Intelligent control based on neuroendocrine system will have a positive impact on the development of traditional control theory, which is very suitable for improving the control quality of complex nonlinear objects [18]. However, there is no relevant report on the research of biological intelligent controller in semi-active suspension of high-clearance sprayers. In this paper, semi-active suspension of light-load high-clearance sprayers is taken as research object, and combined with single-neuron PID control and endocrine regulation mechanism, an intelligent controller of high-clearance sprayer semi-active suspensions based on neuroendocrine algorithm is designed. And the actuator in the high-clearance sprayer suspension is continuous damping control (CDC) damper.

Suspension is a typical strong nonlinear complex variable time-delay system [19]. With the gradual deepening of research on controllable suspension and its control technology, due to the objective existence of time-lag, the inevitable time-lag problem and unexpected instability in controllable suspension systems have become key issues that urgently need to be addressed [20-22]. Chen et al. [23] studied Taylor-LQG method for time-lag suspension systems, which can preferably strengthen the performance of suspension systems. Yu et al. [24] proposed an adaptive fault-tolerant algorithm for time-delay nonlinear feedback system with stochastic faults in the deadband actuator, which applicability is proofed through application examples. Ye et al. [25] proposed a H_∞ robust controller considering response time-lag of magnetorheological dampers, which superiority is proved through experiments. Fu et al. [26] analyzed the effect of time-lag on stability and dynamic performance and designed fuzzy-Smith algorithm, which sensibly strengthened driving safety of vehicles. However, the traditional Smith algorithm is only applicable to fixed time-lag system, which has certain limitations. Kou et al. [27] proposed an adaptive Smith feedback method, which time-lag is a fixed value and cannot get the effect of time-lag dynamic compensation. However, the above studies are all conducted for the suspension

system of the automobile chassis, and the research on the time-lag of the high-clearance sprayer is basically blank. Therefore, it is very necessary to design a semi-active suspension compound control strategy for high-clearance sprayer considering time-lag compensation, smoothness and road-friendliness for improving comprehensive performance of sprayers.

From above analysis, it is known that existing semi-active suspension algorithms for high-clearance sprayers do not meet the actual engineering requirements. Motivated by the need to improve smoothness and road-friendliness of high-clearance sprayers, a novel high-clearance sprayer semi-active suspension controller based on enhanced Smith predictive neuroendocrine algorithm is proposed, which contributions are summarized.

(1) A novel neuroendocrine intelligent controller for high-clearance sprayer is proposed, which effectively improves the spraying effect and ride comfort of high-clearance sprayer.

(2) Combined with enhanced Smith controller, a high-clearance sprayer semi-active suspension controller based on enhanced Smith predictive neuroendocrine is designed, which realized time-lag dynamic compensation of sprayer for the first time.

(3) A comprehensive performance evaluation index of high-clearance sprayer suspension is established, which comprehensively reflect the overall driving performance of high-clearance sprayers. The practicability of the proposed controller is proofed through experiment analysis under different working conditions, which provides a new method for development of suspension intelligent controllers of high-clearance sprayer.

The remainder is organized. In Section 2, time-lag semi-active suspension dynamic model for high-clearance sprayer is presented. In Section 3, the improved Smith predictive neuroendocrine intelligent controller is presented. In Section 4, the experiment results under different operating conditions are presented. In Section 5, the conclusion is presented.

2. Time-lag suspension model of high-clearance sprayer

When establishing the suspension time-lag model, only the influence of the actuator response time-lag on the vibration characteristics is usually considered, the other system time-lag, such as time-lag of calculation, time-lag of transmission all can be eliminated through the software and hardware of the system [28]. 1/4 suspension can better reflect low-frequency vibration characteristics concerned by the ride comfort, and is the basis for studying the high-clearance sprayer suspension. The structure of 1/4 light-load high-clearance sprayer suspension is shown in Fig. 1. In Fig. 1, m_1 is sprung mass, m_2 is unsprung mass, k_1 is suspension stiffness, k_2 is the tire stiffness, c_1 is tire damping, x_1 is sprung mass displacement, x_2 is unsprung mass displacement, and x_q is road excitation.

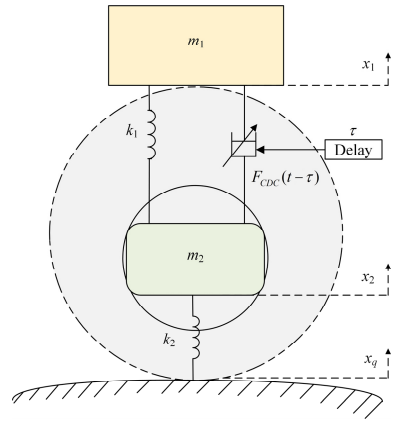

Fig. 1. 1/4 high-clearance sprayer semi-active suspension

Combining the delay differential equation theory, the 1/4 high-clearance sprayer semi-active

suspension time-lag equation as shown in Eq. (1):

$$\begin{cases} m_1\ddot{x}_1(t) + k_1[x_1(t) - x_2(t)] + c_s[\dot{x}_1(t) - \dot{x}_2(t)] - F_{CDC}(t-\tau) = 0, \\ m_2\ddot{x}_2(t) - k_1[x_1(t) - x_2(t)] - c_s[\dot{x}_1(t) - \dot{x}_2(t)] + c_1[\dot{x}_2(t) - \dot{x}_q(t)] \\ \quad + k_t[x_2(t) - x_q(t)] + F_{CDC}(t-\tau) = 0, \\ F_{CDC}(t-\tau) = c_s[\dot{x}_1(t) - \dot{x}_2(t)] + c_r[\dot{x}_1(t-\tau) - \dot{x}_2(t-\tau)]. \end{cases} \tag{1}$$

Among them, c_r is adjustable damping of CDC damper, c_s is base damping of CDC damper, τ is the amount of time-lag, $F_{CDC}(t-\tau)$ is adjustable damping force at the moment of t with time-lag τ. The parameters of the 1/4 high-clearance sprayer suspension are displayed in Table 1 [29], the dynamic critical time-delay calculation method can be referred to the literature [30].

Table 1. Parameters of 1/4 high-clearance sprayer semi-active suspension

Parameters	Value
Sprung mass (kg)	800
Unsprung mass (kg)	300
Suspension stiffness (N/m)	39800
Tire stiffness (N/m)	220000
Base damping (N.s/m)	1000

The state space equation established according to Eq. (1) is displayed in Eq. (2):

$$\begin{cases} \dot{\mathbf{X}} = \mathbf{AX} + \mathbf{BU} + \mathbf{\Gamma W}, \\ \mathbf{Y} = \mathbf{CX} + \mathbf{DU}, \end{cases} \tag{2}$$

where, $\mathbf{X} = [x_2 - x_q, x_1 - x_2, \dot{x}_2, \dot{x}_1]^T$ is system state variable, $\mathbf{A}$ is state matrix, $\mathbf{B}$ is the input matrix, $\mathbf{\Gamma}$ is the perturbation output matrix, $\mathbf{C}$ is the output matrix, $\mathbf{D}$ is the state feedback matrix, and $\mathbf{Y} = [\ddot{x}_1, x_1 - x_2, x_2 - x_q, k_2(x_2 - x_q)]^T$ is the output variable of the system, which can be collated to show that the expression of each matrix in Eq. (2):

$$\mathbf{A} = \begin{bmatrix} 0 & 0 & 1 & 0 \\ 0 & 0 & -1 & 1 \\ \dfrac{-k_2}{m_2} & \dfrac{k_1}{m_2} & \dfrac{-c_1}{m_2} & 0 \\ 0 & \dfrac{-k_1}{m_1} & 0 & 0 \end{bmatrix}, \quad \mathbf{B} = \begin{bmatrix} 0 \\ 0 \\ \dfrac{-1}{m_2} \\ \dfrac{1}{m_1} \end{bmatrix}, \quad \mathbf{C} = \begin{bmatrix} 0 & \dfrac{-k_1}{m_1} & 0 & 0 \\ 0 & 1 & 0 & 0 \\ 0 & 0 & -1 & 1 \\ k_2 & 0 & 0 & 0 \end{bmatrix},$$

$$\mathbf{D} = \begin{bmatrix} \dfrac{1}{m_1} \\ 0 \\ 0 \\ 0 \end{bmatrix}, \quad \Gamma = \begin{bmatrix} -1 \\ 0 \\ \dfrac{c_1}{m_2} \\ 0 \end{bmatrix}$$

The critical time-lag of semi-active suspension system is the critical point at which it transitions from asymptotic stable state to unstable state [31]. According to the existence conditions of solutions to differential equations, the non-zero characteristic equation of Eq. (1) is obtained as shown in Eq. (3):

$$\begin{vmatrix} m_2s^2 + c_re^{-\tau s} + c_ss + k_2 + k_1 & -c_sse^{-\tau s} - k_1 + c_ss \\ -c_sse^{-\tau s} - k_1 + c_ss & m_1s^2 + c_re^{-\tau s} + c_ss + k_1 \end{vmatrix} = 0. \tag{3}$$

The critical condition for system instability is that the characteristic Eq. (3) has pure virtual roots $s = i\omega$ [32, 33]. Substituting $s = i\omega$ into Eq. (3), using Euler's formula to obtain:

$$\begin{cases} m_1 m_2 s^4 - (m_2 k_1 + m_1 k_2 + m_1 k_1) + k_1 k_2 = 0, \\ [k_2 + 5k_1 - (m_1 + m_2)s^2][c_s + c_r(\cos\omega t - \sin\omega t)]\omega = 0. \end{cases} \tag{4}$$

According to Eq. (4), the critical time-lag calculation formula for semi-active suspension system can be obtained:

$$\tau = \frac{\arcsin(\sqrt{2}c_s/2c_r) + \pi/4}{\omega}, \tag{5}$$

where, when the base damping c_s is constant, the critical lag τ decreases with the increase of c_r, when c_r is small enough, the system enters a fully delayed stable state.

Performing Fourier transform on the dynamic equation of the semi-active suspension system with time-lag in Eq. (1) as shown in Eq. (6):

$$\begin{cases} x_1(-\omega^2 m_1 + j\omega c_r + k_1 + j\omega c_r e^{-j\omega\tau}) = x_2(k_1 + j\omega c_s + j\omega c_r e^{-j\omega\tau}), \\ x_2(-\omega^2 m_2 + k_1 + k_2 + j\omega c_s + j\omega c_r e^{-j\omega\tau}) = x_1(k_1 + j\omega c_s + j\omega c_r e^{-j\omega\tau}) + k_2 x_q. \end{cases} \tag{6}$$

According to Eq. (6), the frequency response relationship between BVA, tire dynamic deformation (TDD) indicators and road excitation input is shown in Eqs. (7-8):

$$\left|\frac{\ddot{x}_1}{x_q}\right| = \left|\omega^2 k_2 \frac{A_2}{A_1 A_3 - A^2{}_2}\right|, \tag{7}$$

$$\left|\frac{x_2 - x_q}{x_q}\right| = \left|k_2 \frac{A_1}{A_1 A_3 - A^2{}_2} - 1\right|, \tag{8}$$

where, $A_1 = -\omega^2 m_1 + k_1 + j\omega c_s + j\omega c_r e^{-j\omega\tau}$, $A_2 = k_1 + j\omega c_s + j\omega c_r e^{-j\omega\tau}$, $A_3 = -\omega^2 m_2 + k_1 + k_2 + j\omega c_s + j\omega c_r e^{-j\omega\tau}$.

According to Eqs. (7-8), the response curves of different time-lag on the amplitude frequency characteristics of semi-active suspension systems are obtained, as shown in Fig. 2.

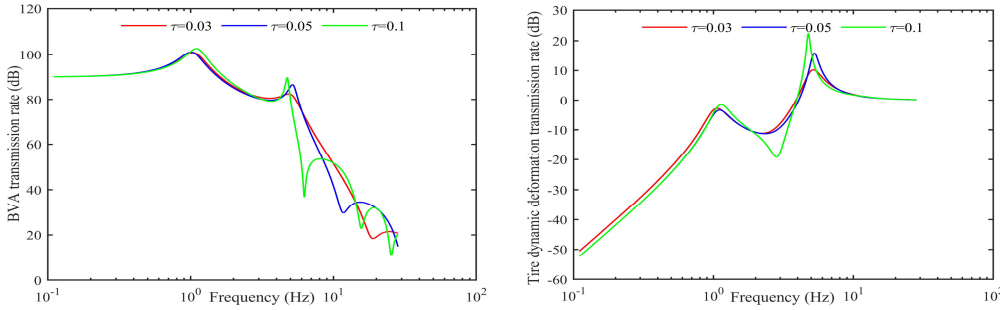

a) b)

Fig. 2. Amplitude frequency response: a) the BVA to road excitation acceleration, b) TDD to road excitation acceleration

According to the analysis in Fig. 2, as the time-lag continues to increase, the amplitude of the first and second principal modes of the semi-active suspension system significantly increases, and the larger the time-lag, the larger the amplitude. The resonance frequency of the first-order principal mode gradually increases, while the resonance frequency of the second-order principal mode gradually decreases. Time-lag mainly affects the first-order principal mode of the suspension, and has a relatively small impact on the second-order principal mode, which means that time-lag mainly affects the smoothness of vehicles.

3. Improved Smith predictive neuroendocrine intelligent controller

3.1. Single-neuron PID controller

The single-neuron serves as the fundamental control unit in neural network systems, exhibiting strong self-adaptation, self-learning ability, which can realize the online self-tuning of system parameters. The single-neuron PID controller has been widely used in industrial control [34]. Through self-learning ability of single-neuron, the dynamic adjustment of the PID controller parameters is achieved, with the aim of improving stability and robustness of systems, its structure is displayed in Fig. 3.

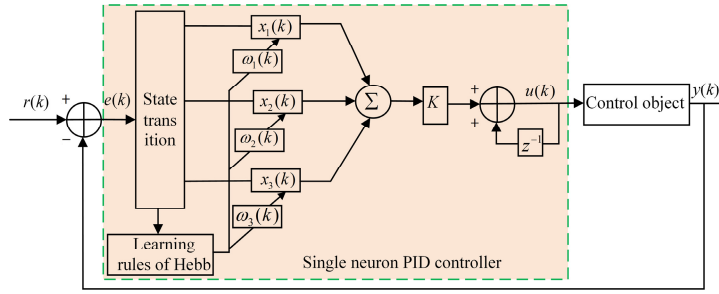

Fig. 3. Single-neuron PID controller

In Fig. 3, $x_1(k)$, $x_2(k)$, $x_3(k)$ are the proportional, integral and differential inputs in PID controller, and the weight coefficients $\omega_1(k)$, $\omega_2(k)$, $\omega_3(k)$ correspond to proportional, integral, differential coefficients, respectively, which are dynamically adjusted to achieve self-learning and self-adaptation of control systems. The output is shown in Eq. (9):

$$u(k) = u(k-1) + K\sum_{i=1}^{3} \omega_i'(k)\, x_i(k). \tag{9}$$

Among them, $\omega_i'(k)$ represents weight coefficient of $x_i(k)$, K is proportion coefficient of neurons, and $K > 0$. $u(k)$ represents input signal to controlled object at time k, where:

$$\begin{cases} e(k) = r(k) - y(k), \\ x_1(k) = e(k), \\ x_2(k) = \Delta e(k) = e(k) - e(k-1), \\ x_3(k) = e(k) - 2e(k-1) + e(k-2), \\ z(k) = e(k), \end{cases} \tag{10}$$

$$\omega_i'(k) = \frac{\omega_i(k)}{\sum_{i=1}^{3} |\omega_i(k)|}. \tag{11}$$

To dynamically adjust weighting coefficients $\omega_i(k)$, this paper adopts the supervised Hebb learning rule for online adjustment [35], which is shown in Eq. (12):

$$\begin{cases} \omega_1(k) = \omega_1(k-1) + \eta_P z(k) u(k) x_1(k), \\ \omega_2(k) = \omega_2(k-1) + \eta_I z(k) u(k) x_2(k), \\ \omega_3(k) = \omega_3(k-1) + \eta_D z(k) u(k) x_3(k). \end{cases} \tag{12}$$

Among them, η_P, η_I, η_D represent proportional, integral and derivative learning rates, respectively.

3.2. Endocrine controller

As the most important male hormone, testosterone plays a significant part in regulating metabolism and growth, which regulation process is displayed in Fig. 4. Hypothalamus secretes Gonadotropin-releasing hormone (GnRH), when pituitary gland is stimulated by GnRH, the pituitary gland secretes luteinizing hormone (LH) and follicle stimulating hormone (FSH), when testis is stimulated by both LH and FSH, the testicular interstitial cells on the testis secrete testosterone (T_e), and the concentration of testosterone in the organism will be fed back to its superiors and its own regulatory glands through a variety of transducers, resulting in a decrease in the secretion of GnRH, LH and FSH, thus causing a decrease in the secretion of T_e in the organism. Through a certain period of internal regulation, changes in hormones can achieve the goal of hormonal balance in the body.

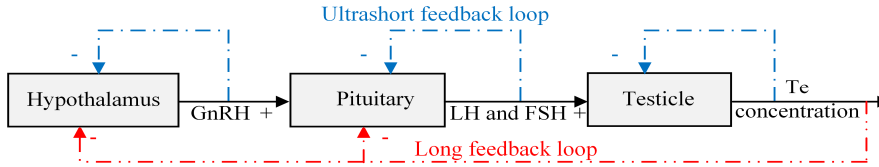

Fig. 4. Testosterone hormone regulatory circuit

The concentration of testosterone in biological fluids is taken as output variable of control systems, hypothalamus unit and pituitary unit in the regulatory circuit are taken as the corresponding system controllers, the normal value of the corresponding hormone concentration in the organism is taken as ideal reference value of control systems, and the secretory tissues of the various glands are taken as the actuators of the control system. The regulatory model of testosterone is a typical two-layer control structure, and the regulatory process of testosterone in Fig. 3 is transformed into an endocrine controller structure in Fig. 5.

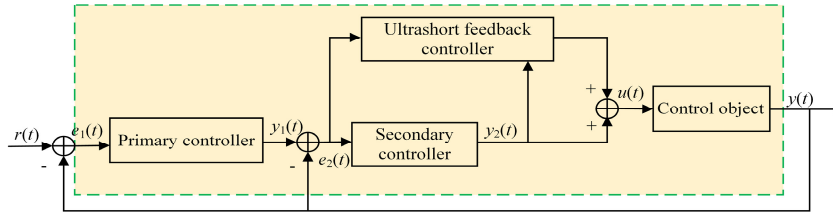

Fig. 5. Endocrine controller based on testosterone secretion regulation

In Fig. 5, $e_1(t)$ and $y_1(t)$ represent deviation and output of primary controller. $e_2(t)$ and $y_2(t)$ represent deviation and output of secondary controller. The feedback signals of primary and secondary controllers are the actual measured values, and the input of secondary controller is error between the output of primary controller and the actual measured values. The primary controller achieves the goal of quickly and stably eliminating control deviations by dynamically changing the expected value of secondary controller. Among them, the primary controller adopts proportional controller and the secondary controller adopts single-neuron PID controller. When system deviation occurs, firstly, the proportional action through the primary controller can quickly adjust the output, and then eliminate deviation quickly and stably through secondary controller.

Traditional control strategies only contain long feedback loops and rarely consider the ultrashort feedback control role of the controller's own output signals. Inspired by the ultrashort feedback mechanism in organisms [36], an ultrashort feedback controller is added to the endocrine controller. On the basis of the generalized law of hormone glands secreting hormones [37], the nonlinear function of the ultra-short feedback controller is designed. Namely, the change rate $\Delta y_2(t)$ of the secondary controller output signal is used as the hormone excitation signal, and

according to the law of Hill's function followed by hormone regulation, the nonlinear feedback processing function of the short feedback controller output signal is shown as Eq. (13):

$$f(\Delta y_2(k)) = ab\left(\frac{|\Delta y_2(k)|^n}{1+(|\Delta y_2(k)|)^n}\right), \tag{13}$$

$$b = \begin{cases} 1, & e_2 \geq 0, \\ -1, & e_2 < 0. \end{cases} \tag{14}$$

Among them, a, n are factor coefficients related to the magnitude, and b is related to the direction.

The output of neuroendocrine intelligent controller is displayed in Eq. (15):

$$u(k) = y_2(k) + f(\Delta y_2(k)). \tag{15}$$

3.3. Improved Smith predictive controller

From the control theory, time-lag is the main reason for the decline or even deterioration of control performance, the larger the time-lag, the more difficult it is to control the system, so time-lag compensation is the key to achieving variable time-delay semi-active suspension control. To improve control performance of nonlinear time-lag systems, Smith put forward a model-based predictive compensation algorithm [38], as shown in Fig. 6. Firstly, the system dynamic response under the action of the perturbation is estimated in advance and compensated by the predictor, so that the controlled quantity which is delayed by τ is fed back to the controller in advance, so that the controller acts in advance, thus accelerating the system regulation process.

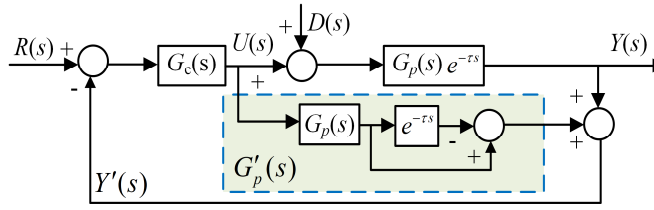

Fig. 6. Smith predictive compensation control

In Fig. 6, $R(s)$ represents the ideal input of the system, $U(s)$ represents controller output, $Y(s)$ represents the system output, $G_c(s)$ represents the controller model, $D(s)$ represents the system disturbance, $G_p(s)e^{-\tau s}$ represents the actual system model with time-lag, andτrepresents the pure time-lag of the system. From Fig. 6, when Smith predictor is not considered, the transfer function between $U(s)$ and $Y(s)$ is shown in Eq. (16):

$$\frac{Y(s)}{U(s)} = G_p(s)e^{-\tau s}. \tag{16}$$

When using Smith predictor, the transfer function between the feedback signal $Y'(s)$ and $U(s)$ is shown in Eq. (17):

$$\frac{Y'(s)}{U(s)} = G_p(s)e^{-\tau s} + G_p'(s). \tag{17}$$

To achieve requirement of time-lag compensation control in the control system, the output signal and feedback signal of the controller have no time-delay, the Eq. (18) must be satisfied:

$$\frac{Y'(s)}{U(s)} = G_p(s)e^{-\tau s} + G_p'(s) = G_p(s). \tag{18}$$

According to Eq. (18), transfer function of Smith predictor is displayed in Eq. (19):

$$G_p'(s) = G_p(s)(1 - e^{-\tau s}). \tag{19}$$

The closed-loop function of control systems is displayed in Eq. (20):

$$\frac{Y(s)}{R(s)} = \frac{G_c(s)G_p(s)e^{-\tau s}}{1 + G_c(s)G_p(s)e^{-\tau s} + G_c(s)G_p(s)(1 - e^{-\tau s})} = \frac{G_c(s)G_p(s)e^{-\tau s}}{1 + G_c(s)G_p(s)}, \tag{20}$$

$$\frac{Y(s)}{D(s)} = \frac{G_p(s)e^{-\tau s} + G_c(s){G^2}_p(s)e^{-\tau s} - G_c(s){G^2}_p(s)e^{-2\tau s}}{1 + G_c(s)G_p(s)}. \tag{21}$$

According to Eq. (20-21), the closed-loop characteristic equations of systems no longer contain pure time-lag link $e^{-\tau s}$. Therefore, the use of Smith predictive control eliminates the time-lag influence on system stability and $e^{-\tau s}$ only delays the control response byτin the time coordinate axis, the process control of controlled system and other indexes are identical to that of the system $G_p(s)$. However, traditional Smith has the problem of over-dependence on the accuracy of the model [39], and it is only applicable to fixed time-lag compensation, and better results can only be obtained when the compensation is the same as the actual time-lag. Since high-clearance sprayer is a complex dynamic system with multiple physical variables and high-order nonlinearity, obtaining an accurate model of the system is extremely difficult, and the semi-active suspension of the sprayer needs to adjust the controllable damping in real time under the complex and variable working conditions, and the system time-lag varies in real time, the traditional Smith algorithm is not applicable to time-varying time-lag compensation for high-clearance sprayer semi-active suspension. Therefore, an improved Smith predictive compensation controller is displayed in Fig. 7.

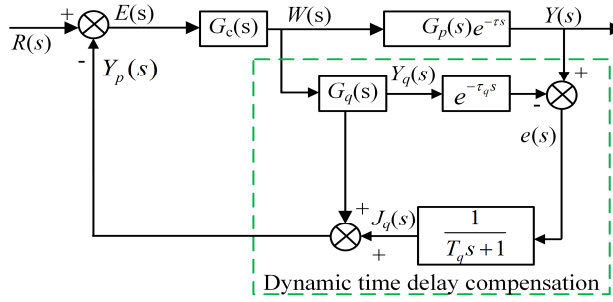

Fig. 7. Improved Smith predictive controller

In Fig. 7, $G_q(s)$ is ideal compensation model, $e^{-\tau_q s}$ is the estimated time-delay, and $G_p(s)e^{-\tau s}$ represents system model with time-lag. When the predictor model matches the actual model perfectly, the time-lag compensator is a conventional Smith controller, which can be used to eliminate the adverse effects of pure time-lag on the stability. A first-order filter is introduced to suppress high-frequency noise and modeling errors. The filter is defined as:

$$F(s) = \frac{1}{T_q s + 1}. \tag{22}$$

Among them, T_q denotes the filter time constant.

The deviation signal is calculated as the difference between the measured system output $Y(s)$ and the predicted output $Y_q(s)e^{-\tau_q s}$, which can be expressed as:

$$e(s) = Y(s) - Y_q(s)e^{-\tau_q s}. \tag{23}$$

The deviation signal is then processed through the first-order filter to attenuate high-frequency disturbances before being used for compensation in the predictor. The filtered deviation signal is further utilized to adjust the compensating term $J_q(s)$. Specifically, $J_q(s)$ acts as a corrective transfer function that compensates for model mismatch and lag estimation errors. By introducing the filtered deviation into the adjustment mechanism, the improved Smith predictor can effectively reduce prediction errors and enhance robustness against disturbances and parameter uncertainties. Namely, the closed-loop feedback signal of the improved Smith compensation method consists of an estimated output $Y_q(s)$ without time-lag and $J_q(s)$ between the estimated output with time-lag and the actual output processed by a first-order filtering process. By using the first-order filter, the improved Smith prediction compensation method can enhance the stability and anti-interference ability of the system, ensuring robustness even in the presence of modeling errors.

Improved Smith predictive compensation controller is combined with the established neuroendocrine intelligent controller to construct the improved Smith neuroendocrine controller (ISNC), which structure is displayed in Fig. 8. 1/4 high-clearance sprayer semi-active suspension obtains the ideal control force of the CDC damper in the neuroendocrine controller, then uses improved Smith algorithm to carry out the time-lag compensation control for ideal control force of the actuator in advance. The control signal can be obtained by the inverse model of CDC damper, then control CDC damper to output the corresponding control force to achieve the purpose of synchronizing the control force with the suspension state and obtain better control effect.

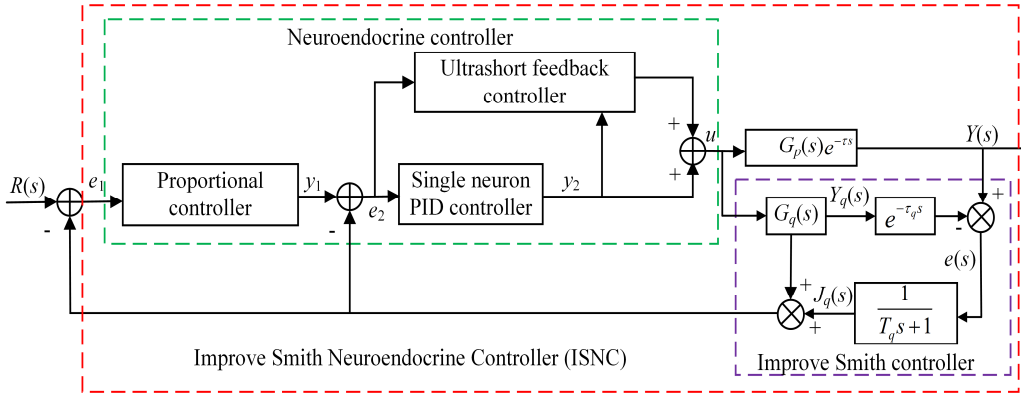

Fig. 8. Improved Smith neuroendocrine controller

4. Simulation verification

Combined with the characteristics of road roughness, the C-level random road is used to simulate the transit transportation condition, and the E-level random road is used to simulate the spraying operation condition in the field [40], and the corresponding random road is generated by the filtered white noise method [41]. Considering the control characteristics of the semi-active suspension system for high-clearance sprayers, set $K = 40$, $\eta_P = 20$, $\eta_I = 15$, $\eta_D = 20$, $a = 10$, $n = 2$, $T_q = 80$ by trial-and-error method. To verify the validity of the ISNC, passive suspension (PS), linear quadratic regulator (LQR) controller and traditional Smith neuroendocrine controller (TSNC) for comparative analysis.

ISSN PRINT 1392-8716, ISSN ONLINE 2538-8460

4.1. Transit transportation conditions

The response of BVA and TDL are displayed in Fig. 9 when high-clearance sprayer running of 40 km/h on the Class C random road, the RMS of the relevant indexes under different control strategies are displayed in Table 2.

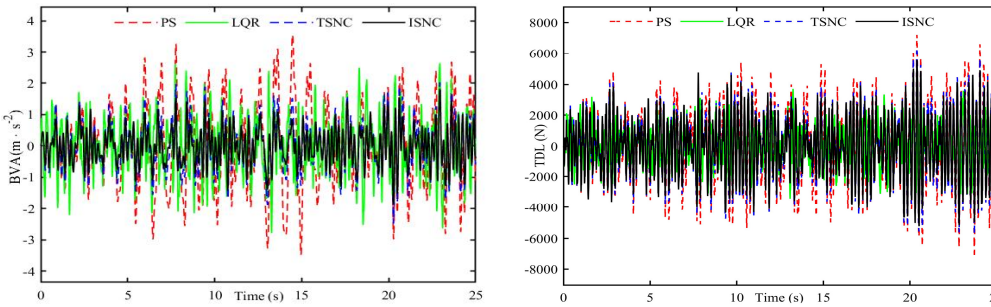

Fig. 9. Response of high-clearance sprayer suspension under transition conditions: a) BVA, b) TDL

Table 2. RMS indicators of high-clearance sprayer suspension under transition conditions

Algorithms	BVA (m/s^2)	SDD (m)	TDL (N)
PS	1.173	0.0233	1998
LQR	0.8966 (↓23.56 %)	0.0053 (↓77.25 %)	1177 (↓41.09 %)
TSNC	0.7065 (↓39.77 %)	0.0144 (↓38.20 %)	1760 (↓11.91 %)
ISNC	0.5256 (↓55.19 %)	0.0120 (↓48.50 %)	1647 (↓17.57 %)

From Fig. 9 and Table 2, compared to PS, RMS of BVA, SDD, TDL indicators under LQR decreased by 23.56 %, 77.25 % and 41.09 %. RMS of BVA, SDD, TDL indicators controlled by TSNC decreased by 39.77 %, 38.20 % and 11.91 %, respectively. However, RMS of BVA, SDD, TDL indicators controlled by ISNC are reduced by 55.19 %, 48.50 % and 17.57 % respectively, and MAX of BVA, SDD, TDL indicators are significantly reduced. The BVA control effect of ISNC is significantly better than that of LQR and TSNC, which effectively improved smoothness of the high-clearance sprayer. The TDL control effect of LQR is significantly better than that of ISNC and TSNC, which effectively improved road-friendliness of the high-clearance sprayer.

4.2. Spray operation conditions

The control effects of different control strategies under variable operating conditions are analyzed when the high-clearance sprayer is spraying at 3 km/h, 6 km/h, 9 km/h, 12 km/h and 15 km/h, respectively, on a Class E random road. Due to the limitation of space, the time-frequency response of BVA and TDL of semi-active suspension systems at 9 km/h are shown in Figure 10, and the MAX and RMS indexes of BVA and TDL controlled by different control strategies under variable operating conditions are displayed in Figs. 11-12.

From Fig. 10, compared to PS, time-frequency domain responses of BVA and TDL controlled by the proposed ISNC under variable operating conditions are significantly reduced, and its control effect with the range of 1-4 Hz is significantly better than that of LQR and TSNC, effectively improved the smoothness and road-friendliness of the vehicle. From Figs. 11-12, compared to PS, MAX and RMS of BVA controlled by TSNC under variable operating conditions are reduced by about 25 % and 30 %. MAX and RMS of TDL controlled by TSNC under variable operating conditions are reduced by about 5 % and 8 %, respectively. Under variable working conditions, MAX and RMS of BVA controlled by ISNC are reduced by about 30 % and 40 % respectively, and MAX and RMS of TDL controlled by ISNC are reduced by about 10 % and 10 % respectively. MAX of SDD controlled by TSNC and ISNC under variable working

conditions meets the control requirements, improves the ride comfort of high-clearance sprayer, and further verifies the practicability of ISNC.

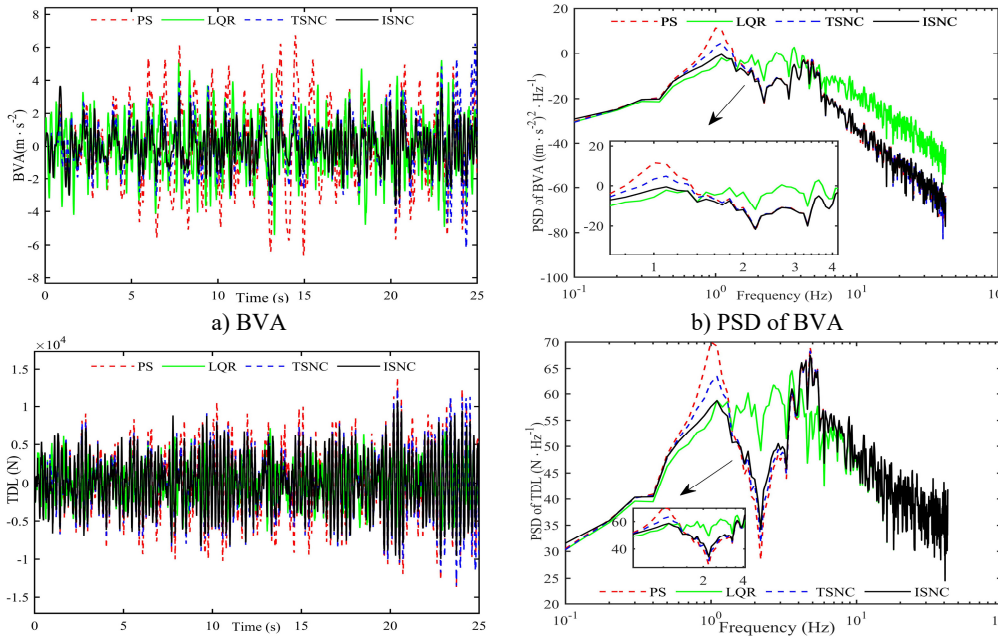

a) BVA b) PSD of BVA

c) TDL d) PSD of TDL

Fig. 10. Time-frequency response of semi-active suspensions at 9 km/h

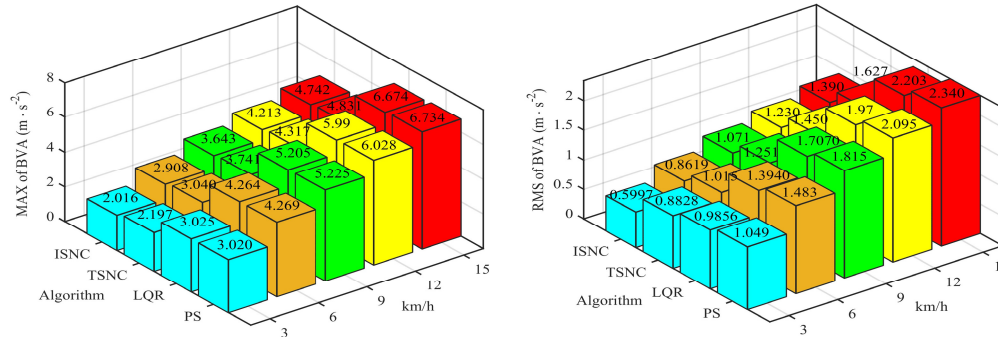

a) MAX of BVA b) RMS of BVA

Fig. 11. BVA controlled by different control strategies under variable operating conditions

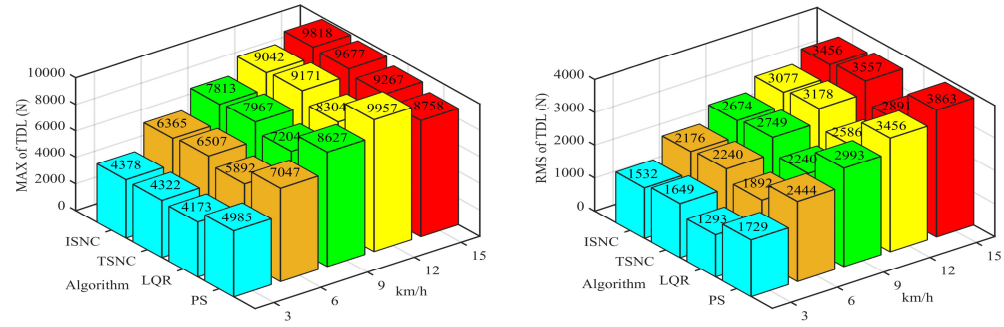

a) MAX of TDL b) RMS of TDL

Fig. 12. TDL controlled by different control strategies under variable operating conditions

ISSN PRINT 1392-8716, ISSN ONLINE 2538-8460

4.3. Adaptability of control strategy

To further verify the adaptability and robustness of ISNC, and in combination with the time variability of the sprung mass during the spraying process of high-clearance sprayers, the sprung mass of sprayers is 800 kg, 900 kg and 1000 kg, respectively, to simulate the no-load (NL), medium load (ML) and full load (FL) working conditions of the sprayer, and speed is 9 km/h. Time-domain response of BVA and TDL under ML is obtained as shown in Fig. 13. The change trend of MAX and RMS value indicators of BVA and TDL under different sprung mass working conditions is shown in Figs. 14-15, respectively.

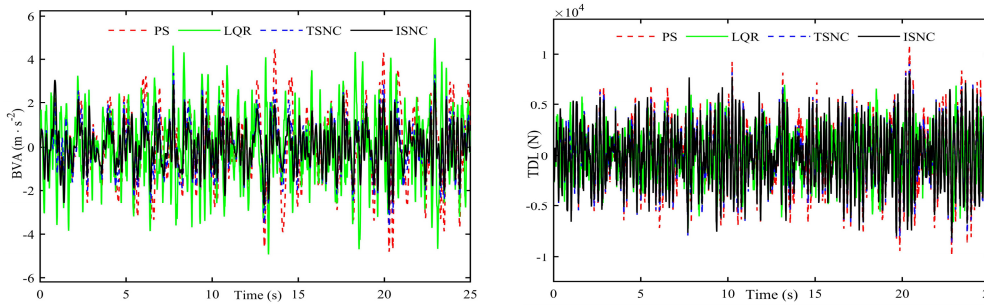

a) BVA b) TDL

Fig. 13. Response of semi-active suspension system under ML condition

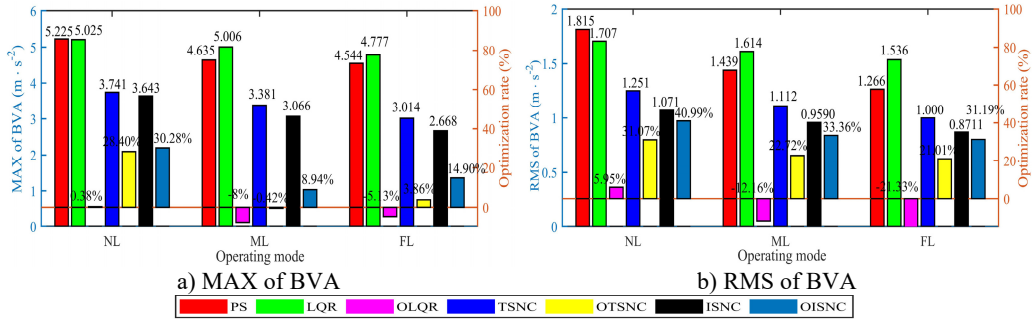

a) MAX of BVA b) RMS of BVA

Fig. 14. BVA of semi-active suspension under variable operating conditions

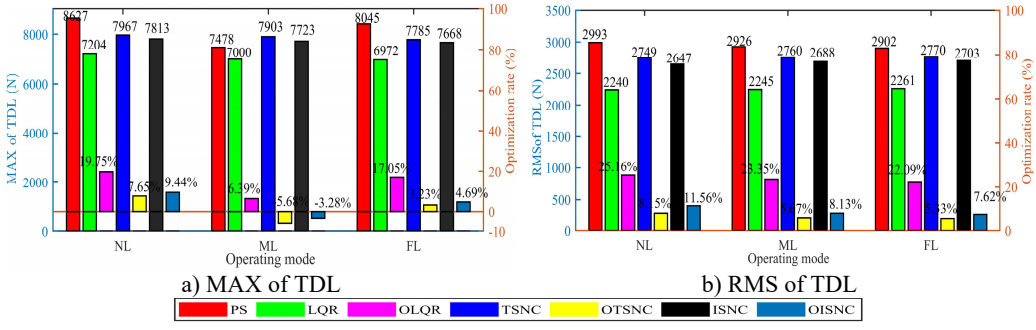

a) MAX of TDL b) RMS of TDL

Fig. 15. TDL of semi-active suspension under variable operating conditions

In Fig. 13, compared with LQR, the BVA indicator controlled by TSNC and ISNC are prominently reduced, effectively reducing the impact of variable time-lag on high-clearance sprayer semi-active suspension, improving ride comfort and road friendliness of high-clearance sprayer. The TDL indicator controlled by LQR are prominently reduced, which control effect is superior to TSNC and ISNC, and effectively reducing the compaction effect of sprayer tires on

soil, thus ensuring the normal growth of crops. The performance of ISNC is superior to TSNC, with strong robustness and working condition adaptability.

From Fig. 14, compared to PS, MAX and RMS of BVA for LQR under NL, ML and FL conditions decreased by 0.38 %, –8.00 %, –5.13 % and 5.95 %, –12.16 %, –21.33 %, respectively. MAX and RMS of BVA controlled by TSNC under NL, ML and FL conditions decreased by 28.40 %, –0.42 %, 3.86 % and 31.07 %, 22.72 %, 21.01 %, respectively, while MAX and RMS of BVA controlled by ISNC under NL, ML and FL conditions decreased by 30.28 %, 8.94 %, 14.90 % and 40.99 %, 33.36 %, 31.19 %, respectively. From Fig. 15, compared to PS, MAX and RMS of TDL for LQR under NL, ML and FL conditions decreased by 19.75 %, 6.39 %, 17.05 % and 25.16 %, 23.35 %, 22.09 %, respectively. MAX and RMS of TDL controlled by TSNC under NL, ML and FL conditions decreased by 7.65 %, –5.68 %, 3.23 % and 8.15 %, 5.67 %, 5.33 %, respectively, MAX and RMS of TDL controlled by ISNC under NL, ML and FL conditions decreased by 9.44 %, –3.28 %, 4.69 % and 11.56 %, 8.13 %, 7.62 %, respectively. Under different spraying conditions, the BVA control effect of TSNC and ISNC is significantly better than LQR, the TDL control effect of LQR is better than TSNC and ISNC. And the control effect of BVA and TDL for ISNC is significantly better than TSNC, which further verifies the effectiveness of the proposed controller, significantly enhances smoothness and road-friendliness of high-clearance sprayer.

4.4. Comprehensive performance

At present, scholars at home and abroad mostly adopt a single objective approach when designing and verifying suspension system vibration control algorithms, such as reducing the RMS of BVA to increase smoothness and reducing the RMS of TDL to increase road-friendliness [42]. However, the single control objective and evaluation index can only improve the driving performance in a certain aspect, without considering the impact of other driving performance, and is not suitable for complex suspension system models and multi-objective control [43]. Therefore, this paper comprehensively considers smoothness and road-friendliness of the high-clearance sprayer suspension, establishes a comprehensive performance evaluation index of high-clearance sprayer suspension, so as to comprehensively reflect the overall driving performance of high-clearance sprayers, which evaluation index is shown in Eq. (24):

$$Q_{CP} = \left(\alpha \sqrt{\frac{Q_{RC}}{Q_{RC-P}}} + \beta \sqrt{\frac{Q_{RF}}{Q_{RF-P}}} \right)^4, \tag{24}$$

where, Q_{RC-P}, Q_{RF-P} respectively represent smoothness and road-friendliness indicators of PS, Q_{RC}, Q_{RF} respectively represent smoothness and road-friendliness indicators of semi-active suspension. α, β respectively represent weight coefficients of smoothness and road friendliness, and $\alpha + \beta = 1$. Since more attention is paid to smoothness in the transit transportation condition and more attention is paid to the road-friendliness in the spraying operation, the results of comprehensive performance evaluation under different performance indexes are obtained by taking $\alpha = 0.5, \beta = 0.5$, as shown in Fig. 16. In Fig. 16, the red part represents the reference plane, which is the comprehensive performance of PS. The part below the reference plane represents the improvement of comprehensive performance, while the part above the reference plane represents the deterioration of comprehensive performance.

Combined with the performance index under transition conditions in Table 2 and Eq. (24), the comprehensive performance evaluation parameters under transition condition are displayed in Table 3.

From Table 3, compared to PS, the ride comfort index Q_{RC} controlled by LQR, TSNC and ISNC decreased by 23.56 %, 39.77 % and 55.19 %, respectively. The road-friendliness index Q_{RF}

controlled by LQR, TSNC, and ISNC decreased by 41.09 %, 11.91 % and 17.57 %, respectively. According to Eq. (24), the comprehensive performance evaluation index Q_{CP} of high-clearance sprayer suspension is obtained. Under transition condition, the comprehensive performance of high-clearance sprayer suspension controlled by LQR, TSNC and ISNC decreases by 54.59 %, 45.98 % and 61.31 %. Due to the use of a fourth power form in the comprehensive performance evaluation criteria, the rewarding and punishing effect of ISNC makes its comprehensive performance superior to both ride comfort and road-friendliness. The ISNC control strategy effectively improves road-friendliness while considering ride comfort, which control effect is superior to LQR and TSNC, further verifying the effectiveness of ISNC.

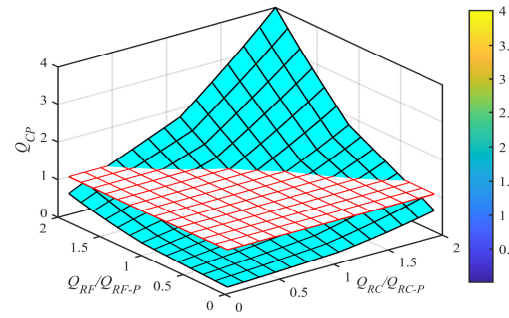

Fig. 16. Trend of comprehensive performance evaluation

Table 3. Comprehensive performance evaluation of high-clearance suspension under transition conditions

Algorithms	Q_{RC}		Q_{RF}		Q_{CP}	
	Value	Optimize	Value	Optimize	Value	Optimize
PS	1.173	–	1998	–	1.0000	–
LQR	0.8966	23.56 %	1177	41.09 %	0.4541	54.59 %
TSNC	0.7065	39.77 %	1760	11.91 %	0.5402	45.98 %
ISNC	0.5256	55.19 %	1647	17.57 %	0.3869	61.31 %

5. Conclusions

To decrease the time-lag influence on the sprayer semi-active suspension, a novel semi-active suspension control strategy based on improved Smith predictive neuroendocrine is designed, and the dynamic time-lag compensation control of sprayer suspension is realized. Firstly, the time-lag dynamic model of high-clearance sprayer semi-active suspension is established, and neuroendocrine controller of semi-active suspension is designed combined with biological regulation mechanism. Then, improved Smith predictive compensation controller is combined with the neuroendocrine controller to design ISNC algorithm. The research results show the performance of ISNC is superior to LQR and TSNC, which effectively improves smoothness and road-friendliness of sprayers, and has strong adaptability and robustness under working conditions. In the future work, the real vehicle test system of high-clearance sprayer will be built, and the real vehicle test of improving Smith predictive neuroendocrine intelligent control strategy under variable working conditions will be carried out, which will lay the foundation for the actual development of semi-active suspension controller of high-clearance sprayer.

Acknowledgements

The authors have not disclosed any funding.

Data availability

The datasets generated during and/or analyzed during the current study are available from the

corresponding author on reasonable request.

Author contributions

Congcong Chen: conceptualization, methodology, writing-original draft. Weiwei Song: methodology, validation. Gang Li: funding acquisition, software. Yuling Ye: writing-review and editing, methodology. Junfeng An: resources, data curation, formal analysis.

Conflict of interest

The authors declare that they have no conflict of interest.

References

[1] L. Lu, J. Zhang, J. Chen, Y. Chen, C. Hu, and J. Cao, "Optimized design of the high clearance sprayer chassis suspension considering tank liquid shaking," (in Chinese), *Transactions of the Chinese Society of Agricultural Engineering*, Vol. 39, No. 10, pp. 15–25, 2023.

[2] C. Hu, Y. Chen, J. Cao, X. Chen, S. Zhang, and J. Chen, "Research on constant speed cruise control of 4WID high ground clearance self-propelled electric sprayer," *Journal of Intelligent Agricultural Mechanization*, Vol. 14, No. 6, p. 902, Jun. 2024, https://doi.org/10.3390/agriculture14060902

[3] F. Yang, G. Yan, and Y. Hao, "Study on the characteristics of steering system for high clearance sprayer based on rigid-flexible coupling simulation model," (in Chinese), *Journal of Jilin University*, Vol. 45, No. 3, pp. 857–863, Mar. 2015, https://doi.org/10.13229/j.cnki.jdxbgxb201503025

[4] Y. Chen, S. Chen, Y. Du, Z. Zhu, E. Mao, and Q. Fu, "Damping characteristics of chassis suspension system of high clearance agricultural machinery based on friction damper," (in Chinese), *Transactions of the Chinese Society of Agricultural Engineering*, Vol. 32, No. 7, pp. 51–57, 2016.

[5] L. Tan et al., "Design and preliminary experiment of track width adjustment system for sprayer based on integral separated fuzzy proportional integral derivative control strategy," *Agriculture*, Vol. 14, No. 8, p. 1247, Jul. 2024, https://doi.org/10.3390/agriculture14081247

[6] Y. Qi, S. Luo, Y. Zheng, H. Jing, J. Wang, and H. Dai, "Stability analysis of high speed trains based on active anti-yaw damper control with electro-hydraulic actuator," *Vehicle System Dynamics*, Vol. 423114, pp. 1–27, Dec. 2026, https://doi.org/10.1080/00423114.2026.2621043

[7] P. R. Sanchez and H. Zhang, "Precision spraying using variable time delays and vision-based velocity estimation," *Smart Agricultural Technology*, Vol. 5, p. 100253, Oct. 2023, https://doi.org/10.1016/j.atech.2023.100253

[8] S. Li and W. Wang, "Adaptive backstepping robust control of nonlinear spray boom system," *Journal of Advanced Agricultural Technologies*, Vol. 6, No. 4, pp. 246–252, Jan. 2019, https://doi.org/10.18178/joaat.6.4.246-252

[9] X. Yin, J. An, X. Wang, Y. Wang, J. Li, and C. Jin, "Design and test of automatic beam leveling system for high-clearance sprayer," (in Chinese), *Transactions of the Chinese Society for Agricultural Machinery*, Vol. 53, No. 2, pp. 98–105, Feb. 2023, https://doi.org/10.1177/09544070241280403

[10] T. Xue, W. Li, Y. Du, E. Mao, and H. Wen, "Adaptive fuzzy sliding mode control of spray boom active suspension for large high clearance sprayer," (in Chinese), *Transactions of the Chinese Society of Agricultural Engineering*, Vol. 34, No. 21, pp. 47–56, 2023.

[11] F. Yang et al., "Research on a variable universe control method and the performance of large sprayer active suspension based on an artificial fish swarm algorithm-back propagation fuzzy neural network," *Agriculture*, Vol. 14, No. 6, p. 811, Jun. 2024, https://doi.org/10.3390/agriculture14060811

[12] L. Cui, X. Xue, and F. Le, "Adaptive robust precision control of an active spray boom suspension with disturbance estimation," *Journal of Vibration and Control*, Vol. 29, No. 3-4, pp. 925–941, Mar. 2021, https://doi.org/10.1177/10775463211055273

[13] Y. Nie, H. Xu, G. Cai, L. Gao, Y. Zhao, and F. Wu, "Design of wide-area damping controller based on immune system," *Power System Technology*, Vol. 44, No. 12, pp. 4713–4721, 2020.

[14] B. Liu, M. Xu, L. Gao, J. Yang, and X. Di, "A hybrid approach for high-dimensional optimization: Combining particle swarm optimization with mechanisms in neuro-endocrine-immune systems," *Knowledge-Based Systems*, Vol. 253, p. 109527, Oct. 2022, https://doi.org/10.1016/j.knosys.2022.109527

[15] F. Ding et al., "Gain self-adjusting single neuron PID control method and experiments for longitudinal relative position of harvester and transport vehicle," *Computers and Electronics in Agriculture*, Vol. 213, p. 108215, 2023, https://doi.org/10.1016/j.compag.2023.108215

[16] D. Su et al., "Single-neuron PID UAV variable fertilizer application control system based on a weighted coefficient learning correction," *Agriculture*, Vol. 12, No. 7, p. 1019, Jul. 2022, https://doi.org/10.3390/agriculture12071019

[17] Y. Jin, D. Yu, Z. Chen, M. Jiang, and X. He, "Endocrine LQR control strategy and its application in vibration suppression by active suspensions," (in Chinese), *Journal of Vibration and Shock*, Vol. 35, pp. 49–54, Oct. 2016, https://doi.org/10.13465/j.cnki.jvs.2016.10.008

[18] C. Kong and W. Zhou, "A single neuron PID intelligent controller based on neuron endocrine," (in Chinese), *Control Engineering of China*, Vol. 23, No. 2, pp. 265–268, 2016, https://doi.org/10.14107/j.cnki.kzgc.140037

[19] Y. Liu, L. Yang, and X. Hao, "Singularity-free finite-time tracking control of active suspension systems with dead-zone output," (in Chinese), *Control and Decision*, Vol. 40, No. 7, pp. 1–7, 2025, https://doi.org/10.13195/j.kzyjc.2024.1140

[20] J. Duan, X. Huang, and Z. Chen, "Robust compensation control for active suspension subject to input delay," (in Chinese), *Journal of Vibration and Shock*, Vol. 39, No. 24, pp. 254–277, Dec. 2020, https://doi.org/10.13465/j.cnki.jvs.2020.24.035

[21] S. Shao, C. Ren, D. Jin, and T. Yan, "Stability, bifurcation and chaos of nonlinear active suspension system with time delay feedback control," (in Chinese), *Journal of Vibration and Shock*, Vol. 40, No. 7, pp. 281–290, Jul. 2021, https://doi.org/10.13465/j.cnki.jvs.2021.07.038

[22] L. Chen, "Time delay on semi-active suspension and control system," (in Chinese), *Journal of Mechanical Engineering*, Vol. 42, No. 1, p. 130, Jan. 2006, https://doi.org/10.3901/jme.2006.01.130

[23] S. Chen, G. Zu, M. Yao, and X. Zhang, "Taylor series-LQG control for time delay compensation of magneto-rheological semi-active suspension," (in Chinese), *Journal of Vibration and Shock*, Vol. 36, No. 8, pp. 190–196, Aug. 2017, https://doi.org/10.13465/j.cnki.jvs.2017.08.030

[24] X. Yu, H. Pan, W. Sun, and H. Gao, "Reliable control for a class of nonlinear time-delay systems against actuator faults with application to suspension control," *IEEE/ASME Transactions on Mechatronics*, Vol. 24, No. 6, pp. 2498–2507, Dec. 2019, https://doi.org/10.1109/tmech.2019.2948477

[25] Q. Ye, X. Qiang, Y. Zhang, R. Wang, R. Ding, and Y. Cai, "H∞ control and experimental study of magnetorheological semi-active suspension with actuator response delay," *Journal of Mechanical Engineering*, Vol. 60, No. 18, p. 276, 2024, https://doi.org/10.3901/jme.2024.18.276

[26] W. Fu, H. Pang, K. Liu, and F. Liu, "A study on time delay stability analysis and fuzzy smith control strategy for semi-active suspension system with magnetorheological fluids damper," (in Chinese), in *Proceedings of the 2016 China Society of Automotive Engineers Annual Meeting*, 2016.

[27] F. Kou, H. Zhang, J. Xu, H. Tian, and X. Peng, "Adaptive smith feedback time delay control of active suspension with electro hydrostatic actuator," (in Chinese), *Journal of Vibration, Measurement and Diagnosis*, Vol. 42, No. 5, pp. 864–870, May 2022, https://doi.org/10.16450/j.cnki.issn.1004-6801.2022.05.004

[28] Y. Guo, G.-F. Xu, and C.-Y. Duan, "Research on time-delayed vibration reduction control of 1/4 vehicle semi-active suspension system with three degrees of freedom," *Advances in Mechanical Engineering*, Vol. 16, No. 9, pp. 1–16, Sep. 2024, https://doi.org/10.1177/16878132241273541

[29] X. Wu, J. Qin, Y. Du, Z. Song, Y. Chen, and B. Xie, "Experiments of vibration control for active pneumatic suspension system in high clearance self-propelled sprayer," (in Chinese), *Transactions of the Chinese Society for Agricultural Machinery*, Vol. 49, No. 6, pp. 60–67, 2018.

[30] Y. Zhao, "Time lag of magnetorheological damper semi-active suspensions," *Journal of Mechanical Engineering*, Vol. 45, No. 7, p. 221, Jan. 2009, https://doi.org/10.3901/jme.2009.07.221

[31] Y. Qi, J. Wang, H. Dai, S. Luo, Y. Zheng, and H. Jing, "Research on the effect of vertical installation angle and layout of anti-yaw damper on the dynamic performance of high-speed EMUs," *Journal of Vibration and Control*, Vol. 11, pp. 1–15, Feb. 2026, https://doi.org/10.1177/10775463261424829

[32] F. Kou, "Design and test of vehicle semi-active suspension with magnetorheological damper," (in Chinese), *Transactions of the Chinese Society for Agricultural Machinery*, Vol. 47, No. 4, pp. 1–8, 2016.

[33] G. Ji, S. Li, G. Feng, Z. Li, and X. Shen, "Time-delay compensation control and stability analysis of vehicle semi-active suspension systems," *Mechanical Systems and Signal Processing*, Vol. 228, p. 112414, Apr. 2025, https://doi.org/10.1016/j.ymssp.2025.112414

[34] Y. Zhang, "Research on stability of aviation inspection equipment based on improved single neuron PID control," (in Chinese), *Control Engineering of China*, Vol. 32, No. 3, pp. 394–399, Mar. 2025, https://doi.org/10.14107/j.cnki.kzgc.20220543

[35] M. Zhou et al., "Development of a depth control system based on variable-gain single-neuron PID for rotary burying of stubbles," *Agriculture*, Vol. 12, No. 1, p. 30, Dec. 2021, https://doi.org/10.3390/agriculture12010030

[36] B. Liu and Y. Ding, "A two-level controller based on the modulation principle of testosterone release," (in Chinese), *Journal of Shanghai Jiaotong University*, No. 5, pp. 822–824, May 2006, https://doi.org/10.16183/j.cnki.jsjtu.2006.05.026

[37] L. S. Farhy, "Modeling of oscillations in endocrine networks with feedback," in *Methods in Enzymology*, Vol. 384, Elsevier, 2004, pp. 54–81, https://doi.org/10.1016/s0076-6879(04)84005-9

[38] J. Zhang, *Adaptive Suspension System for Tank Armored Vehicles*. National Defense Industry Press, 2014.

[39] T. Zhang, X. Fang, F. Liu, and Z. Li, "Anti-disturbance control of refrigeration system based on improved smith predictor compensation," (in Chinese), *Control Engineering of China*, Vol. 27, No. 7, pp. 1204–1209, Jul. 2020, https://doi.org/10.14107/j.cnki.kzgc.170999

[40] Z. Xu, X. Xue, L. Cui, and X. Zhou, "Review on farmland ground vibration spectrum," (in Chinese), *Journal of Chinese Agricultural Mechanization*, Vol. 37, No. 7, pp. 251–255, 2016, https://doi.org/10.13733/j.jcam.issn.2095-5553.2016.07.055

[41] F. Kou, Q. Jing, Y. Gao, and J. Wu, "A novel endocrine composite fuzzy control strategy of electromagnetic hybrid suspension," *IEEE Access*, Vol. 8, pp. 211750–211761, Jan. 2020, https://doi.org/10.1109/access.2020.3039845

[42] D. Huang, B. Wang, H. Liu, and J. Zhang, "Research on assessment method of vibration control feature of suspension system of vehicle," *Journal of Ordnance Equipment Engineering*, Vol. 42, No. 3, pp. 114–118, 2021.

[43] Z. Liu, H. Cai, T. Guo, X. Liu, Y. Bai, and C. Qu, "Monitoring-based evaluation of wind-induced vibration and travel comfort of long-span suspension bridge," *Structural Control and Health Monitoring*, Vol. 2025, No. 1, p. 9962003, 2025, https://doi.org/10.1155/stc/9962003

Congcong Chen is pursuing a Ph.D. degree in the Key Laboratory of Road and Traffic Engineering, Ministry of Education, Tongji University, Shanghai, China. She is currently an Associate Professor with Department of Rail Transportation, Shandong Jiaotong University. Her research interests include intelligent control, vehicle dynamics and control.

Weiwei Song received his Ph.D. degree, Tongji University, in 2025. His research interests include intelligent control, vehicle dynamics and control.

Gang Li, Assistant to the General Manager of Jinan Rail Transit Group, chief data engineer, doctoral candidate, and Mount Taishan industrial leader in Shandong Province. His research direction is: research on cloud data intelligence integration technology, line network command center, and subway informatization intelligence.

Yuling Ye is a Professor of College of Transportation Engineering, Tongji University. She is also a member of the Science and Technology Committee of the Shanghai Municipal Transportation Commission, a member of the Shanghai Railway Society, and a reviewer for academic journals such as the Journal of Railways, Tongji Journal, and Urban Rail Transit Research.

Junfeng An is the Senior Engineer at Jinan Rail Transit Group Co., Ltd., with research interests in cloud data intelligence fusion technology, line network command center, artificial intelligence and its empowering applications in subways, urban rail vision and intelligent agents, etc.